RSC Advances

PAPER

View Article Online
View Journal | View Issue

Cite this: *RSC Adv.*, 2021, **11**, 15675

Synthesis and biological evaluation of indazole derivatives as anti-cancer agents†

Wei Wei,‡[a] Zhihao Liu,‡[a] Xiuli Wu,[a] Cailing Gan,[a] Xingping Su,[a] Hongyao Liu,[a] Hanyun Que,[a] Qianyu Zhang,[b] Qiang Xue,[a] Lin Yue,[a] Luoting Yu *[a] and Tinghong Ye *[a]

Received 11th February 2021
Accepted 20th April 2021

DOI: 10.1039/d1ra01147b

rsc.li/rsc-advances

Several FDA approved small molecule anti-cancer drugs contain indazole scaffolds. Here, we report the design, synthesis and biological evaluation of a series of indazole derivatives. *In vitro* antiproliferative activity screening showed that compound **2f** had potent growth inhibitory activity against several cancer cell lines (IC_{50} = 0.23–1.15 μM). Treatment of the breast cancer cell line 4T1 with **2f** inhibited cell proliferation and colony formation. **2f** dose-dependently promoted the apoptosis of 4T1 cells, which was connected with the upregulation of cleaved caspase-3 and Bax, and downregulation of Bcl-2. **2f** also decreased the mitochondrial membrane potential and increased the levels of reactive oxygen species (ROS) in 4T1 cells. Additionally, treatment with **2f** disrupted 4T1 cells migration and invasion, and the reduction of matrix metalloproteinase metalloproteinase-9 (MMP9) and increase of tissue inhibitor matrix metalloproteinase 2 (TIMP2) were also observed. Moreover, **2f** could suppress the growth of the 4T1 tumor model without obvious side effects *in vivo*. Taken together, these results identified **2f** as a potential small molecule anti-cancer agent.

1. Introduction

Cancer is one of the most common causes of death and thus is a significant public health burden. The International Agency for Research on Cancer estimated that there were 19.3 million new cases of cancer globally in 2020, mainly due to female breast cancer, lung cancer, and colorectal cancer, which each accounted for ≥10% of the total cases.[1] In addition, the same report estimated that 10.0 million cancer associated-deaths occurred in 2020.[1] Despite major advances in targeted therapies such as immunotherapy,[2] gene therapy,[3] and small molecule drugs,[4] for relapsed or refractory cancers, many of them still lack effective treatment strategies. Metastasis, an important contributor to poor prognosis, also challenges the existing therapies and hinders blocking of cancer progression although the knowledge of underlying mechanisms is growing.[5] Thus, it remains problematic to improve the efficacy of therapeutic regimens, and there is an urgent need to develop more treatment options to control the progression of cancer.

An indazole motif can be applied as not only a functional substituent but also the scaffold to small molecule drugs. Indazole-containing bioactive molecules have pharmacological effects on a wide range of diseases,[6–8] including infectious, inflammatory, neurodegenerative disease and cancer.[9–11] In particular, some indazole derivatives that are developed as kinase inhibitors, have significant anti-cancer activity *in vitro* and *in vivo*. For instance, the multi-kinase inhibitor pazopanib (**1-1**, Fig. 1),[12,13] the c-Met inhibitor merestinib (**1-2**),[14–16] the tropomyosin receptor kinases/proto-oncogene tyrosine-protein kinase ROS1/anaplastic lymphoma kinase inhibitor entrectinib (**1-3**),[17] and the vascular endothelial growth factor receptor/platelet-derived growth factor receptor inhibitor axitinib (**1-4**)[18,19] are approved for the treatment of different cancer types. Furthermore, the fibroblast growth factor receptor inhibitor LY2874455 (**1-5**)[20,21] and the polo-like kinase 4 inhibitor CFI-400945 (**1-6**)[22–24] are investigated in clinical trials of acute myeloid leukemia (in combination with merestinib, NCT03125239)[25] and breast cancer (NCT03624543),[26] respectively (Fig. 1). Additionally, indazole derivatives have various anti-cancer mechanisms besides inhibiting kinase signaling pathways.[27–29] The effective anti-cancer activity of these small molecules prompted us to further design and characterize indazole derivatives as potential therapeutic agents.

To enrich our compound library for screening of anti-cancer agents, we focused on building novel molecules bearing an indazole motif as the scaffold. The effect of a hydrophobic group at the indazole C6 position has already been elucidated

[a]*Sichuan University-University of Oxford Huaxi Joint Centre for Gastrointestinal Cancer, State Key Laboratory of Biotherapy and Cancer Center, West China Hospital, Sichuan University, Chengdu, Sichuan, 610041, China. E-mail: yeth1309@scu.edu.cn; yuluot@scu.edu.cn*

[b]*Research Center for Public Health & Preventive Medicine, West China School of Public Health & Healthy Food Evaluation Research Center, West China Fourth Hospital, Sichuan University, Chengdu, Sichuan, 610041, China*

† Electronic supplementary information (ESI) available. See DOI: 10.1039/d1ra01147b

‡ These authors contributed equally to this work.

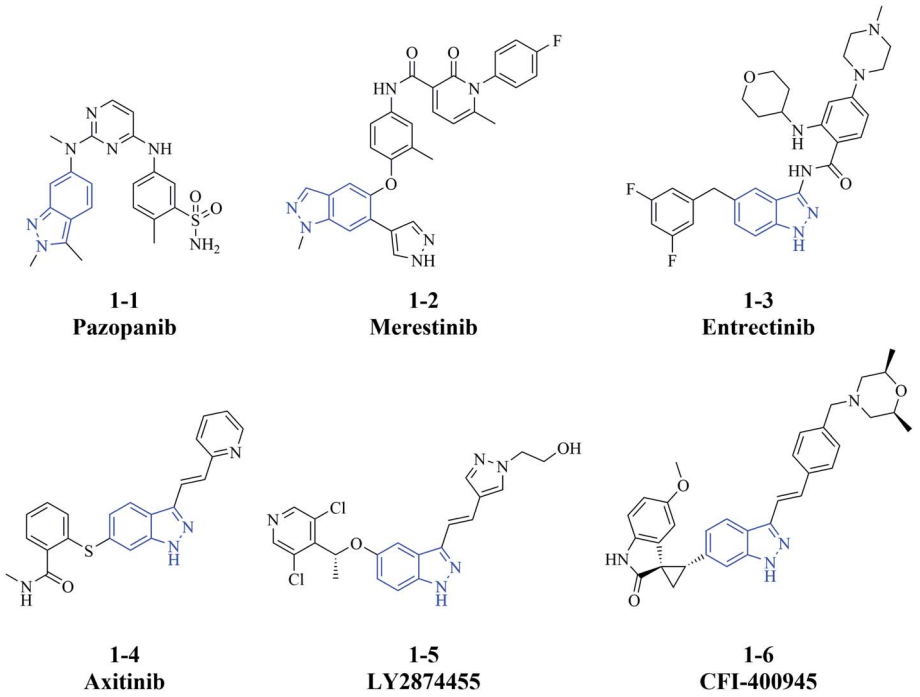

Fig. 1 Structures of kinase inhibitors containing an indazole moiety.

by compounds found in some reports and our previous work, and some of them also have a hydrophilic group at the C3 position like **1-6**.[23,30–35] In this study, we investigated whether exchanging the groups at C3 and C6 would retain their anti-cancer activities. Thus, we synthesized a series of compounds in which a hydrophobic group based on substituted phenyl was linked to the indazole C3 position (R_2) and a hydrophilic group was introduced at indazole C6 (R_1; Fig. 2).

2. Results and discussion

2.1 Chemistry

The synthetic routes of our compounds, **2a–2p**, are shown in Scheme 1. The Heck coupling between 1-bromo-3,5-dimethoxybenzene and 4,4,5,5-tetramethyl-2-vinyl-1,3,2-dioxaborolane produced intermediate **2-1**. Then, **2-1** was dissolved in DMF and reacted with *N*-chlorosuccinimide at 85 °C to afford **2-2**. Intermediate **2-3** was prepared from the iodination of 6-bromo-1*H*-indazole, and reacted with **2-1** or **2-2** through Suzuki coupling to give key intermediates **2-4** and **2-5**, respectively. The target products **2a–2i** and **2k** were obtained from reactions between **2-4** or **2-5** and corresponding boronic acid pinacol esters. The hydrogenation of compound **2f** generated compound **2p**. Compounds **2j** and **2l–2n** were synthesized by another synthesis route (Scheme 2). The preparation of intermediates **2-6–2-9** were conducted through Suzuki coupling between (1*H*-indazol-6-yl)boronic acid and corresponding halides. **2-6–2-9** reacted with iodine in the presence of K_2CO_3 to afford key intermediates **2-10–2-13** respectively. Reactions between intermediates **2-1** and **2-10–2-13** produced target compounds **2j** and **2l–2n**, respectively.

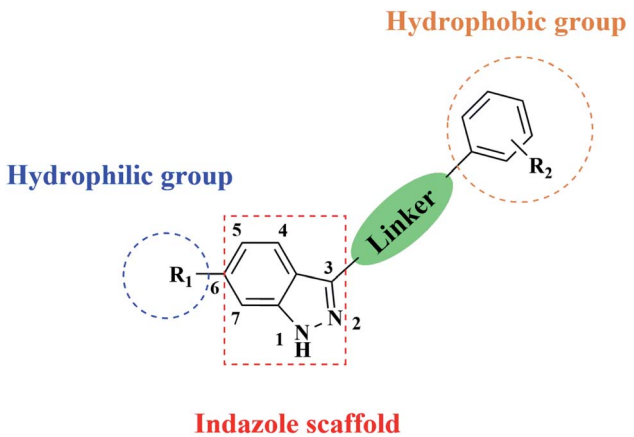

Fig. 2 Structure of our indazole derivatives.

2.2 Antiproliferative activities screening *in vitro*

To evaluate the anti-cancer activities of synthesized compounds, we first examined their ability to inhibit the proliferation of several cell lines representative of cancers with high morbidity; namely, A549 lung cancer cells, HepG2 hepatocellular carcinoma cells, MCF-7 breast cancer cells, and HCT116 colorectal cancer cells, all of which are of human origin. We also examined the mouse breast cancer cell line 4T1, which has a propensity to metastasize. We found that most compounds displayed moderate inhibitory activities against all five cancer cell lines (Table 1). Compounds **2a–2n** all contained (*E*)-3,5-dimethoxystyryl at indazole C3, allowing us to investigate the structure–activity relationship of R_1 substituents. When R_1 was substituted by 4-(4-methylpiperazin-1-yl)phenyl, compound **2a** exhibited unobvious inhibitory activities against A549, 4T1

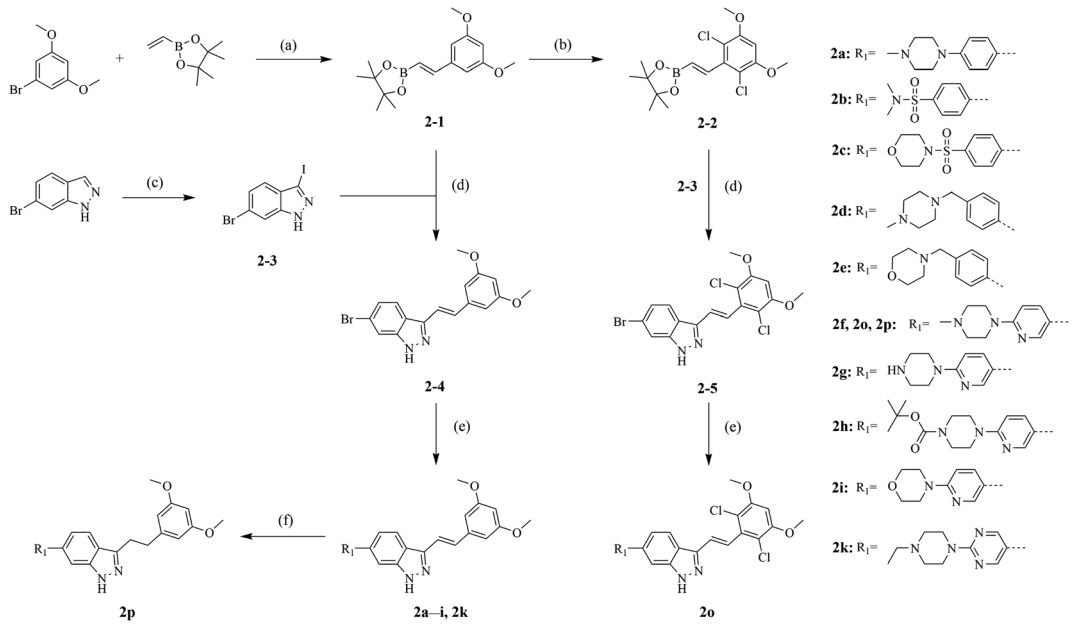

Scheme 1 General procedures for the synthesis of compounds **2a–2i**, **2k** and **2o–2p**. (a) $Pd_2(dba)_3$, DIPEA, P(*t*-Bu)$_3$·HBF_4, toluene, 95 °C, 6 h, 78%; (b) *N*-chlorosuccinimide, DMF, 85 °C, 5 h, 47%; (c) iodine, KOH, DMF, r.t., 3 h, 71%; (d) Pd(dppf)Cl_2, Cs_2CO_3, dioxane/H_2O, 100 °C, 8 h, 46–67%; (e) Pd(dppf)Cl_2, K_2CO_3, dioxane/H_2O, 95 °C, 8 h, 17–31%; (f) H_2, Pd/C, methanol, r.t., overnight, 57%.

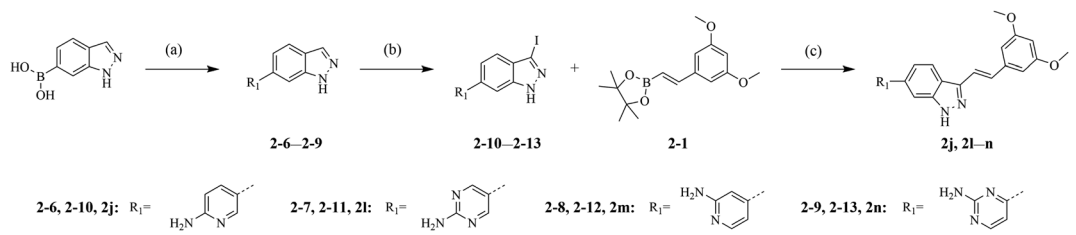

Scheme 2 General procedures for the synthesis of compounds **2j** and **2l–2n**. (a) Pd(dppf)Cl_2, K_2CO_3, dioxane/H_2O, 100 °C, overnight, 56–62%; (b) iodine, K_2CO_3, DMF, 65 °C, 10 h, 80–88%; (c) Pd(dppf)Cl_2, Cs_2CO_3, dioxane/H_2O, 100 °C, 8 h, 12–30%.

Table 1 Antiproliferative activities of compounds **2a–2p**

	Antiproliferative activity[a] (IC_{50}, μM)				
Compd	A549	4T1	HepG2	MCF-7	HCT116
2a	>10	>10	>10	1.15 ± 0.13	4.89 ± 0.29
2b	6.59 ± 1.11	0.91 ± 0.09	>10	1.10 ± 0.04	7.97 ± 1.42
2c	8.06 ± 1.53	1.49 ± 0.19	>10	1.01 ± 0.28	8.63 ± 1.85
2d	1.40 ± 0.22	0.46 ± 0.02	1.16 ± 0.21	0.25 ± 0.01	2.46 ± 0.27
2e	3.90 ± 1.01	1.70 ± 0.43	5.99 ± 1.91	1.01 ± 0.09	4.96 ± 1.52
2f	0.95 ± 0.12	0.23 ± 0.03	0.80 ± 0.05	0.34 ± 0.02	1.15 ± 0.10
2g	1.57 ± 0.31	0.64 ± 0.11	1.90 ± 0.35	0.79 ± 0.15	3.00 ± 0.72
2h	>10	2.62 ± 0.65	9.59 ± 1.14	2.10 ± 0.32	8.28 ± 1.40
2i	3.95 ± 0.78	0.97 ± 0.09	9.52 ± 1.07	1.06 ± 0.18	>10
2j	0.88 ± 0.09	>10	8.44 ± 1.29	>10	3.51 ± 0.86
2k	1.50 ± 0.17	0.20 ± 0.06	2.20 ± 0.53	0.78 ± 0.23	2.88 ± 0.24
2l	1.23 ± 0.38	3.42 ± 0.49	9.41 ± 1.12	8.22 ± 1.06	8.50 ± 1.25
2m	4.16 ± 0.58	3.45 ± 0.39	9.62 ± 1.58	3.28 ± 0.57	7.85 ± 1.03
2n	8.39 ± 1.23	9.15 ± 1.60	9.35 ± 1.74	7.56 ± 1.31	>10
2o	2.10 ± 0.36	0.59 ± 0.08	5.16 ± 0.67	0.79 ± 0.14	3.31 ± 0.66
2p	3.22 ± 0.61	1.15 ± 0.46	8.77 ± 1.41	1.69 ± 0.48	4.88 ± 0.63
Doxorubicin	6.50 ± 1.33	0.98 ± 0.16	0.62 ± 0.03	0.75 ± 0.26	0.19 ± 0.07

[a] Data were the mean ± SD from three independent tests.

and HepG2 cell lines even at a relatively high concentration (IC_{50} > 10 μM), but the proliferation of MCF-7 and HCT116 cells was inhibited by **2a** with IC_{50} values of 1.15 μM and 4.89 μM, respectively. Replacing 4-methylpiperazin-1-yl of **2a** with *N*,*N*-dimethylsulfonamide (**2b**) or 4-sulfonylmorpholine (**2c**) improved the potencies against A549 and 4T1 cells, while placing (4-methylpiperazin-1-yl)methyl or 4-methylmorpholine at the *para*-position of the phenyl (**2d** and **2e**, respectively) maintained or enhanced the activities against all five cell lines, indicating that introducing a sulfonyl or methylene group into phenyl at R_1 was tolerated.

Compared with **2a**, the pyridyl analogue **2f** displayed improved antiproliferative activity, especially against 4T1, HepG2, and MCF-7 cells (IC_{50} values, 0.23 μM, 0.80 μM, and 0.34 μM, respectively). In contrast, either no substitution (**2g**) or a bulky substituent (**2h**) at the piperazinyl N4 position reduced the suppression of cell growth compared with **2f**, implying that suitable size of alkyl substituent at that position was favorable. **2i**, containing 4-morpholine at the pyridyl C2 position, was also inferior to **2f**, but an amino at that position (**2j**) dramatically reduced the antiproliferative activity against all cell lines except A549 (IC_{50} = 0.88 μM). Changing the R_1 substituent to 2-(4-ethylpiperazin-1-yl)pyrimidine (**2k**) only maintained the activity compared with **2f** against 4T1 cells. Similar to **2j**, an amino substituent at pyrimidine C2 position (**2l**) also significantly decreased the activity against all cell lines except A549, suggesting that **2j** and **2l** might have distinct mechanisms of action compared with the other synthesized indazole derivatives. Moving the amino group to the *meta*-position of indazole (**2m** and **2n**) did not improve their potencies compared with **2f**.

To investigate R_2 substitutions, we retained 6-(4-methylpiperazin-1-yl)pyridin-3-yl at the indazole C6 position. Adding chlorine to 3,5-dimethoxystyryl (**2o**) led to a reduction in potency compared with **2f**, and a similar effect was observed when the linker was transformed from vinyl to ethyl (**2p**). Based on the analysis of structure–activity relationship, **2f**, with optimum antiproliferative efficacy *in vitro*, was selected for further evaluation.

2.3 The effects of 2f on 4T1 cell proliferation

To validate the inhibitory activity of **2f** on cancer cell growth and proliferation, we performed the MTT assay and colony formation assay. As shown in Fig. 3A, **2f** decreased 4T1 cell proliferation in a dose- and time-dependent manner. In addition, exposure to **2f** significantly inhibited colony formation of 4T1 cells, and treatment with **2f** at 1.25 μM led to a complete inhibition (Fig. 3B and C), confirming that **2f** had a strong cytostatic effect on 4T1 cells.

2.4 The effects of 2f on 4T1 cell apoptosis

To determine whether the antiproliferative activity of **2f** was associated with activation of the programmed cell death pathways, we examined 4T1 cell apoptosis using the annexin V-FITC/propidium iodide (PI) dual-labeling flow cytometry assay. After **2f** treatment for 24 h, we observed a dose-dependent increase in the percentage of apoptotic cells from 3.7% in the presence of **2f** at 0 μM to 53.2% in the presence of **2f** at 5 μM (Fig. 4A).

To further investigate the pro-apoptotic effect of **2f**, expression of the pro-apoptotic proteins Bax and cleaved caspase-3 and the anti-apoptotic protein Bcl-2 was examined by western blot analysis. As shown in Fig. 4B, incubation of 4T1 cells with **2f** decreased the expression of Bcl-2 and increased that of cleaved caspase-3 and Bax, suggesting that **2f** might induce apoptosis *via*

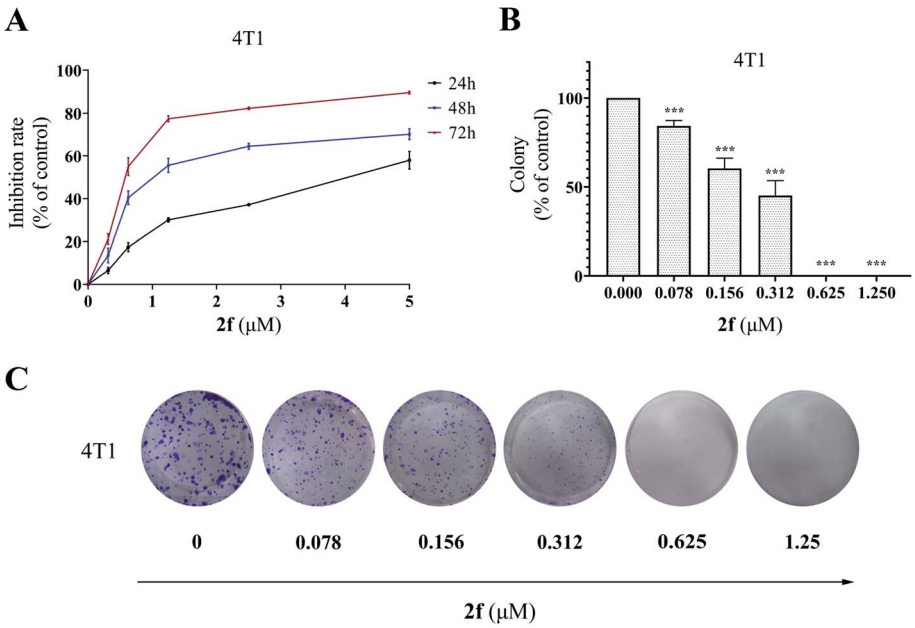

Fig. 3 Effects of **2f** on 4T1 breast cancer cells. (A) MTT proliferation assay performed after incubation of cells for 1–3 days with the indicated concentrations of **2f**. (B, C) Colony formation measured after incubation of cells for 10 days with the indicated concentrations of **2f**. Data were the mean ± SD. ***p < 0.001.

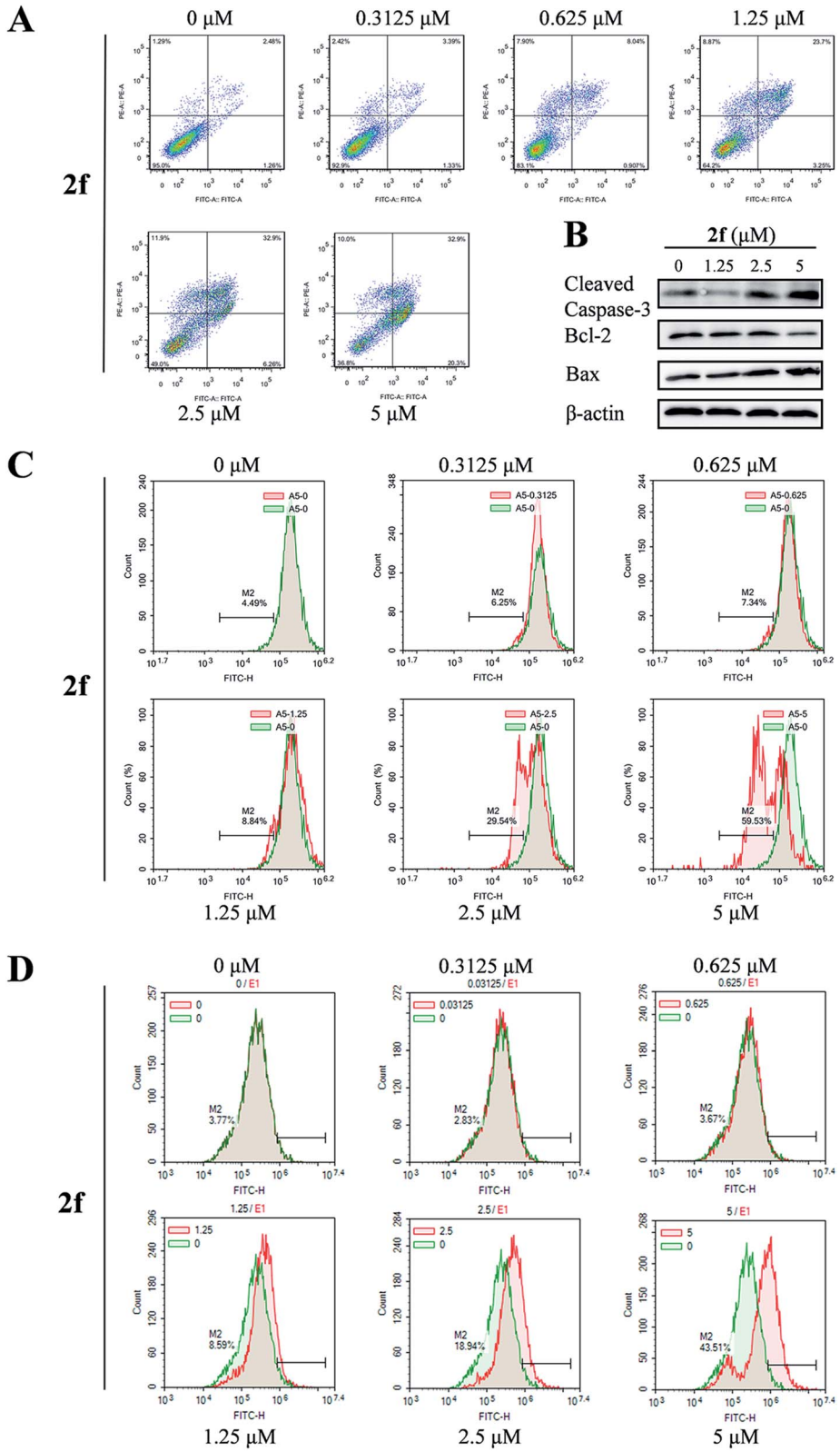

Fig. 4 Effects of **2f** on cell apoptosis. (A) Flow cytometric assay of apoptosis performed by annexin V-FITC/PI dual staining of cells after incubation with the indicated concentrations of **2f** for 24 h. (B) Western blot analysis of cleaved caspase-3, Bcl-2, Bax, and β-actin (loading control) after incubation of cells with **2f** for 24 h. (C) **2f** decreased the mitochondrial membrane potential ($\Delta\Psi$m) in 4T1 cells. 4T1 cells were treated with various concentrations of **2f** for 24 h and then stained with 5 μg ml^{-1} Rh123 to detect the change of $\Delta\Psi$m by FCM. (D) **2f** increased the levels of ROS in 4T1 cells. After treatment with various concentrations of **2f** for 24 h, 4T1 cells were incubated with 10 μM DCFH-DA, and then the ROS levels were measured by DCF fluorescence using FCM.

the mitochondrial apoptotic pathway. Then we measured the effect of **2f** on the mitochondrial membrane potential ($\Delta\Psi$m) of 4T1 cells by a flow cytometric assay using a green fluorochrome Rh123. As shown in Fig. 4C, **2f** caused a dose-dependent loss of $\Delta\Psi$m potential. We also detected ROS levels using the redox-sensitive fluorescent dye 2′,7′-dichlorodihydrofluorescein diacetate (DCFH-DA), and exposure to **2f** resulted in a dose-dependent increase of ROS levels (Fig. 4D). These results implied that the inhibition of 4T1 cells viability after treatment with **2f** was mediated by the mitochondria-mediated apoptotic pathway.

2.5 The effects of 2f on 4T1 cell migration and invasion

To evaluate the potential of **2f** for retarding cell migration and invasion, we performed Transwell assays on 4T1 cells. As shown in Fig. 5A and B, **2f**-treated 4T1 cells exhibited significant and dose-dependent reductions in migration and invasion, and similar results were obtained when migration was evaluated by wound-healing assays. We investigated whether the levels of matrix metalloproteinase metalloproteinase-9 (MMP9) and tissue inhibitor of matrix metalloproteinase 2 (TIMP2), which were considered to be correlated with cell migration and invasion, were affected by **2f** treatment. Western blot analysis demonstrated that **2f** diminished MMP9 levels and increased TIMP2 levels in 4T1 cells (Fig. 5C). Taken together, these findings demonstrated that **2f** restrained the migration and invasion of 4T1 cells.

2.6 Anti-tumor activity of 2f *in vivo*

Next, a preliminary assessment of the anti-tumor activity of **2f** *in vivo* was performed in a mice model. 4T1 tumor-bearing mice were treated with **2f** at doses of 12.5 mg kg^{-1} and 25 mg kg^{-1} once daily. As shown in Fig. 6A and B, **2f** dose-dependently suppressed tumor growth compared with the control treatment without any significant effect on body weights. Considering that tumor volumes are sometimes not very accurate, photographs of tumor size at the end of *in vivo* study were also presented in Fig. S1.† We performed immunohistochemical staining to investigate the underlying mechanism of **2f** anti-tumor activity in this 4T1 model. Notably, tumors from **2f**-treated mice exhibited reduced expression of the cell proliferation marker Ki67 and of MMP9, while expression of cleaved caspase-3 was increased (Fig. 6C). Routine analyses of blood samples and microscopic examination of the major organs of the treated mice revealed no obvious abnormalities in blood markers or morphology of the heart, liver, spleen, lung, and kidney (Fig. S2 and S3†). These results indicated that **2f** potentially reduces the growth of 4T1 breast tumors by promoting cell apoptosis, and that **2f** has an acceptable safety profile in mice. We noted that the effect of **2f** on tumor growth *in vivo* was modest, which was probably due to suboptimal administration route or dosage, and another possibility was that the tumor was too large at the beginning of administration. Further study will be necessary to enhance the anti-tumor and anti-metastatic activities of **2f** *in vivo*.

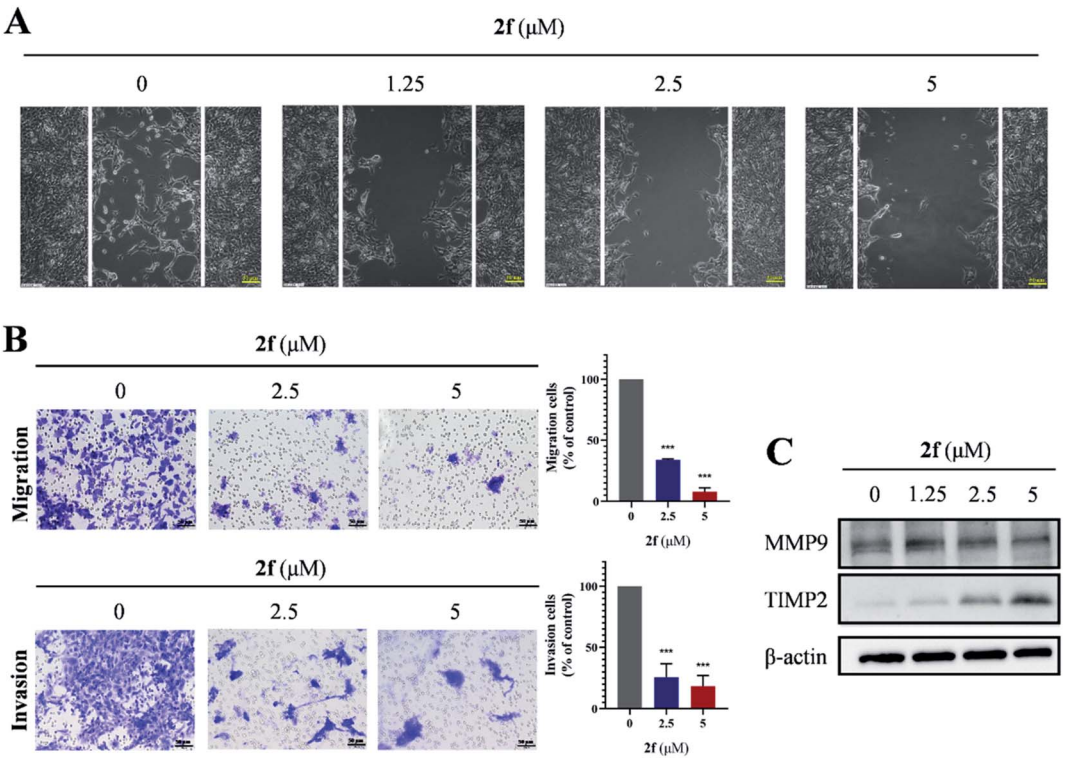

Fig. 5 Effects of **2f** on cell migration and invasion. (A) Cells were seeded in 6 well culture plates, and the cell monolayer was wounded manually. Then, the images were taken after treated with **2f** for 24 h. The scale bar is 50 μm. (B) Images of cells (left) and quantification of data (right) from Transwell migration assays (upper panels) and invasion assays (lower panels) after 24 h treatment of cells with **2f**. The scale bar is 50 μm. (C) Western blot analysis of MMP9, TIMP2, and β-actin (loading control) after incubation of cells with **2f** for 24 h. Data were the mean ± SD. ***p < 0.001.

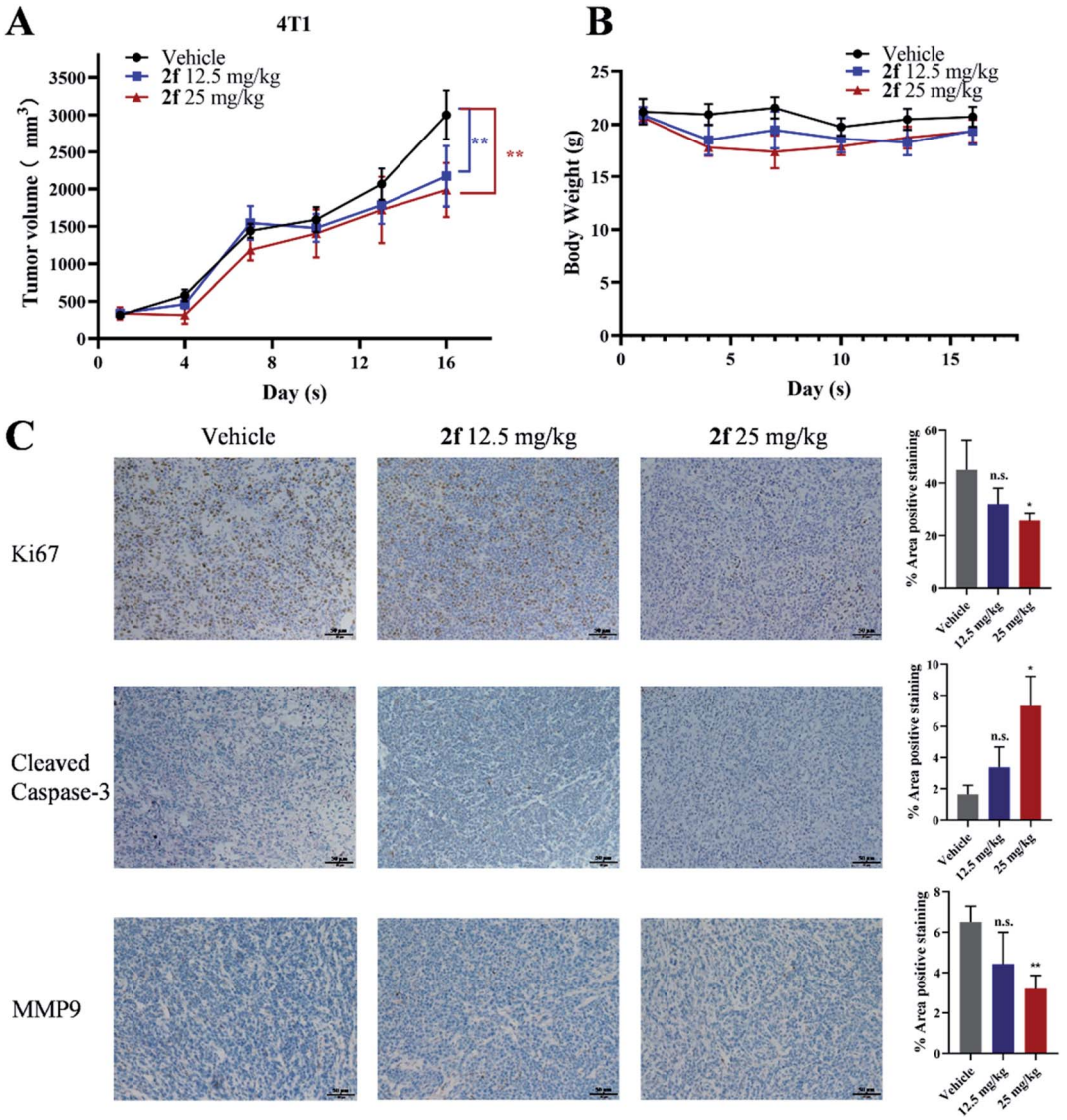

Fig. 6 Anti-tumor effects of **2f** *in vivo*. (A–C) Groups of female BALB/c mice (n = 5/group) were subcutaneously injected with 4T1 cells and received intraperitoneally injection (i.p.) of **2f** 12.5 mg kg^{-1}, 25 mg kg^{-1} or vehicle, respectively once daily for 16 days. (A) Tumor volumes. (B) Body weights. (C) Immunohistochemical staining of Ki67, cleaved caspase-3, and MMP9 in sections of tumors. The scale bar is 50 μm. Data were the mean ± SD, n.s. not significant, *p < 0.05, **p < 0.01.

3. Conclusion

In summary, we designed and synthesized a series of indazole derivatives. **2f**, which was identified as the most potent compound, inhibited cell proliferation and colony formation, as well as migration and invasion *in vitro*. Treatment with **2f** also promoted apoptosis *via* the ROS-mitochondrial apoptotic pathway. Additionally, **2f** suppressed tumor growth in the 4T1 mouse model without obvious side effects. Moreover, Swiss Target Prediction tool was applied to predict the potential target for **2f**, and the results pointed to some tyrosine kinases. However, **2f** only had moderate inhibitory activities against those kinases with inhibition rate <30% at 1 μM (data not shown), which implied that **2f** is probably more like a multi-target inhibitor than a specific kinase inhibitor. Thus, further studies are required to elucidate the precise targets and mechanisms of anti-cancer activity of **2f**, which enable extensive optimization of this compound. Besides, the evaluation of anti-cancer activity in mice xenograft models is also warranted. Overall, **2f** will serve as a potential lead for developing anti-cancer agents.

4. Experimental section

4.1 Chemistry

All commercially available reagents were used without further purification or dried, unless otherwise specified. Thin layer chromatography was carried out on silica gel plates GF254. Column chromatography was performed with silica gel (200–300 mesh). NMR spectra were recorded on a Bruker AV-400

spectrometer with tetramethylsilane (TMS) as an internal standard. The chemical shifts δ and coupling constants J were in ppm and Hz units, respectively. The intermediates were confirmed by Bruker amazon SL LRMS, and the target compounds were identified by Waters Q-TOF Premier HRMS, with ESI ion source. Target compounds were of >95% purity, which was analyzed on a Dionex Ultimate 3000 HPLC, with a Kromasil C18 reversed-phase column (4.6 mm × 250 mm, 5 μm).

4.1.1 Preparation of intermediates 2-1–2-5

*4.1.1.1 (E)-2-(3,5-Dimethoxystyryl)-4,4,5,5-tetramethyl-1,3,2-dioxaborolane (**2-1**).* To a solution of 1-bromo-3,5-dimethoxybenzene (20 mmol, 1.0 equiv.) in dried toluene (60 mL) was added $Pd_2(dba)_3$ (1 mmol, 5 mol%), P(*t*-Bu)$_3\cdot HBF_4$ (2 mmol, 10 mol%), DIPEA (40 mmol, 2.0 equiv.) and 4,4,5,5-tetramethyl-2-vinyl-1,3,2-dioxaborolane (22 mmol, 1.1 equiv.). Then the mixture was stirred at 95 °C under N_2 atmosphere. After 6 h the reaction was monitored by TLC. The solvent was removed under vacuum. To the residue was added water, and extracted with ethyl acetate. The organic layer was dried over anhydrous sodium sulfate and concentrated. The intermediate **2-1** was obtained by column chromatography as a pale-yellow solid (yield 78.1%). MS *m*/*z* (ESI): 291.2 $[M + H]^+$, ^{1}H NMR (400 MHz, DMSO-d_6) δ 7.94 (d, J = 8.0 Hz, 2H), 7.72 (d, J = 8.0 Hz, 2H), 7.37 (d, J = 18.4 Hz, 1H), 6.31 (d, J = 18.5 Hz, 1H), 3.86 (s, 3H), 1.26 (s, 12H).

*4.1.1.2 (E)-2-(2,6-Dichloro-3,5-dimethoxystyryl)-4,4,5,5-tetramethyl-1,3,2-dioxaborolane (**2-2**).* *N*-Chlorosuccinimide (10 mmol, 2.0 equiv.) was added to the solution of compound **2-1** (5 mmol, 1.0 equiv.) in DMF (15 mL). Then the mixture was stirred at 85 °C under N_2 atmosphere. After 5 h the reaction was monitored by TLC. The solvent was removed under vacuum. To the residue was added water, and extracted with ethyl acetate. The organic layer was dried and concentrated. The intermediate **2-2** was obtained by column chromatography as an offwhite solid (yield 47.2%). MS *m*/*z* (ESI): 359.1 $[M + H]^+$; ^{1}H NMR (400 MHz, DMSO-d_6) δ 7.20 (d, J = 18.8 Hz, 1H), 6.89 (s, 1H), 5.98 (d, J = 18.8 Hz, 1H), 3.92 (s, 6H), 1.26 (s, 12H).

*4.1.1.3 6-Bromo-3-iodo-1H-indazole (**2-3**).* To a solution of 6-bromo-1*H*-indazole (10 mmol, 1.0 equiv.) in DMF was added KOH (20 mmol, 2.0 equiv.). Then the solution of I_2 (15 mmol, 1.5 equiv.) in DMF (8 mL) was added dropwise into mixture, and stirred at room temperature for 3 h. After that, the reaction mixture was poured into the aqueous solution of $Na_2S_2O_4$ and K_2CO_3, with a white solid precipitated. The solid was filtered and dried to give intermediate **2-3** as a white solid (yield 71.2%). MS *m*/*z* (ESI): 322.9 $[M + H]^+$, ^{1}H NMR (400 MHz, DMSO-d_6) δ 13.62 (s, 1H), 7.82 (d, J = 1.5 Hz, 1H), 7.40 (d, J = 8.6 Hz, 1H), 7.33 (dd, J = 8.6, 1.6 Hz, 1H).

*4.1.1.4 (E)-6-Bromo-3-(3,5-dimethoxystyryl)-1H-indazole (**2-4**).* The intermediates **2-1** (2.4 mmol, 1.2 equiv.), **2-3** (2 mmol, 1.0 equiv.), Pd(dppf)Cl_2 (0.1 mmol, 5 mol%) and cesium carbonate (3 mmol, 1.5 equiv.) were added to a mixed solvent of water and dioxane (1 : 4, 30 mL). Then the mixture was stirred at 100 °C under N_2 atmosphere. After 8 h the reaction was monitored by TLC. The solvent was evaporated under reduced pressure. The residue was dissolved in dichloromethane and methanol, and filtered with silica. The filtrate was concentrated and purified by column chromatography to afford **2-4**. Pale-yellow solid (yield 67.5%). MS *m*/*z* (ESI): 359.1 $[M + H]^+$.^{1}H NMR (400 MHz, DMSO-d_6) δ 13.28 (s, 1H), 8.18 (d, J = 8.6 Hz, 1H), 7.77 (d, J = 1.6 Hz, 1H), 7.63–7.41 (m, 2H), 7.33 (dd, J = 8.7, 1.7 Hz, 1H), 6.91 (d, J = 2.3 Hz, 2H), 6.44 (t, J = 2.2 Hz, 1H), 3.80 (s, 6H).

*4.1.1.5 (E)-6-Bromo-3-(2,6-dichloro-3,5-dimethoxystyryl)-1H-indazole (**2-5**).* The preparation of intermediate **2-5** is the same as **2-4**. Yellow solid (yield 46.2%). MS *m*/*z* (ESI): 427.1 $[M + H]^+$; ^{1}H NMR (400 MHz, DMSO-d_6) δ 13.25 (s, 1H), 8.03 (d, J = 8.6 Hz, 1H), 7.82 (d, J = 1.6 Hz, 1H), 7.46–7.30 (m, 3H), 6.93 (s, 1H), 3.96 (s, 6H).

4.1.2 General procedure for the preparation of 2a–2i, 2k and 2o

*4.1.2.1 The intermediates **2-4** or **2-5** (0.5 mmol, 1.0 equiv.).* Pd(dppf)Cl_2 (0.1 mmol, 5 mol%), potassium carbonate (1 mmol, 2.0 equiv.) and corresponding boronic acid pinacol esters (0.6 mmol, 1.2 equiv.) were added to a mixed solvent of water and dioxane (1 : 4, 15 mL). Then the mixture was stirred at 95 °C under N_2 atmosphere. After 8 h the reaction was monitored by TLC. The solvent was evaporated under reduced pressure. The residue was dissolved in ethyl acetate, and washed with water. The organic layer was dried over anhydrous sodium sulfate and concentrated. The crude products were purified by preparative thin layer chromatography to give target compounds.

*4.1.2.2 (E)-3-(3,5-Dimethoxystyryl)-6-(4-(4-methylpiperazin-1-yl)phenyl)-1H-indazole (**2a**).* Pale-yellow solid (yield 21.1%). HRMS (ESI-TOF) *m*/*z* calcd for $C_{28}H_{30}N_4O_2$ $[M + H]^+$: 455.2443, found: 455.2449; ^{1}H NMR (400 MHz, DMSO-d_6) δ 13.14 (s, 1H), 8.21 (d, J = 8.5 Hz, 1H), 7.68–7.60 (m, 3H), 7.57 (d, J = 16.7 Hz, 1H), 7.51–7.42 (m, 2H), 7.04 (d, J = 8.7 Hz, 2H), 6.92 (d, J = 2.2 Hz, 2H), 6.44 (t, J = 2.2 Hz, 1H), 3.81 (s, 6H), 3.21 (d, J = 4.9 Hz, 4H), 2.47 (t, J = 5.0 Hz, 4H), 2.23 (s, 3H); ^{13}C NMR (101 MHz, DMSO-d_6) δ 161.16, 150.92, 142.69, 142.56, 139.73, 138.96, 130.80, 129.88, 128.07, 121.78, 121.64, 120.57, 119.87, 115.97, 107.06, 104.82, 100.57, 55.73, 55.02, 48.27, 46.26.

*4.1.2.3 (E)-4-(3-(3,5-Dimethoxystyryl)-1H-indazol-6-yl)-N,N-dimethylbenzenesulfonamide (**2b**).* Pale-yellow solid (yield 31.0%). HRMS (ESI-TOF) *m*/*z* calcd for $C_{25}H_{25}N_3O_4S$ $[M + Na]^+$: 486.1459, found: 486.1458; ^{1}H NMR (400 MHz, DMSO-d_6) δ 13.36 (s, 1H), 8.34 (d, J = 8.5 Hz, 1H), 8.05 (d, J = 8.3 Hz, 2H), 7.92–7.81 (m, 3H), 7.66–7.56 (m, 2H), 7.50 (d, J = 16.6 Hz, 1H), 6.93 (d, J = 2.2 Hz, 2H), 6.45 (d, J = 2.2 Hz, 1H), 3.82 (s, 6H), 2.68 (s, 6H); ^{13}C NMR (101 MHz, DMSO-d_6) δ 161.17, 145.20, 142.73, 142.31, 139.63, 137.15, 134.07, 130.23, 128.71, 128.49, 122.15, 121.39, 121.06, 120.96, 109.30, 104.91, 100.66, 55.74, 38.08.

*4.1.2.4 (E)-4-((4-(3-(3,5-Dimethoxystyryl)-1H-indazol-6-yl) phenyl)sulfonyl)morpholine (**2c**).* Pale-yellow solid (yield 27.3%). HRMS (ESI-TOF) *m*/*z* calcd for $C_{27}H_{27}N_3O_5S$ $[M + Na]^+$: 528.1564, found: 528.1569; ^{1}H NMR (400 MHz, DMSO-d_6) δ 13.38 (s, 1H), 8.35 (d, J = 8.5 Hz, 1H), 8.09–8.04 (m, 2H), 7.90–7.81 (m, 3H), 7.64–7.57 (m, 2H), 7.50 (d, J = 16.7 Hz, 1H), 6.94 (d, J = 2.2 Hz, 2H), 6.45 (t, J = 2.2 Hz, 1H), 3.82 (s, 6H), 3.66 (t, J = 4.7 Hz, 4H), 2.99–2.90 (m, 4H); ^{13}C NMR (101 MHz, DMSO-d_6) δ 161.17, 145.56, 142.73, 142.29, 139.63, 137.08, 133.69, 130.24, 128.84, 128.60, 122.16, 121.39, 121.10, 120.99, 109.37, 104.91, 100.66, 65.79, 55.74, 46.39.

*4.1.2.5 (E)-3-(3,5-Dimethoxystyryl)-6-(4-((4-methylpiperazin-1-yl)methyl)phenyl)-1H-indazole (**2d**).* Light grey solid (yield 24.8%). HRMS (ESI-TOF) *m*/*z* calcd for $C_{29}H_{32}N_4O_2$ $[M + H]^+$:469.2599, found: 469.2603; ^{1}H NMR (400 MHz, DMSO-d_6) δ 13.23 (s, 1H), 8.27 (d, J = 8.5 Hz, 1H), 7.77–7.67 (m, 3H), 7.58 (d, J = 16.7 Hz, 1H), 7.54–7.38 (m, 4H), 6.92 (d, J = 2.3 Hz, 2H), 6.44 (t, J = 2.3 Hz, 1H), 3.81 (s, 6H), 3.51 (s, 2H), 2.38 (d, J = 21.4 Hz, 8H), 2.17 (s, 3H); ^{13}C NMR (101 MHz, DMSO-d_6) δ 161.17, 139.68, 139.49, 138.89, 138.13, 130.03, 129.97, 128.35, 127.43, 121.80, 121.61, 120.99, 120.38, 108.24, 104.85, 100.60, 62.12, 55.74, 55.11, 52.89, 46.05.

*4.1.2.6 (E)-4-(4-(3-(3,5-Dimethoxystyryl)-1H-indazol-6-yl) benzyl)morpholine (**2e**).* Pale-yellow solid (yield 22.3%). HRMS (ESI-TOF) *m*/*z* calcd for $C_{28}H_{29}N_3O_3$ $[M + H]^+$: 456.2283, found: 456.2281; ^{1}H NMR (400 MHz, DMSO-d_6) δ 13.23 (s, 1H), 8.27 (d, J = 8.5 Hz, 1H), 7.72 (d, J = 7.8 Hz, 3H), 7.59 (d, J = 16.7 Hz, 1H), 7.53–7.39 (m, 4H), 6.92 (d, J = 2.3 Hz, 2H), 6.44 (t, J = 2.2 Hz, 1H), 3.81 (s, 6H), 3.60 (t, J = 4.6 Hz, 4H), 3.52 (s, 2H), 2.39 (t, J = 4.6 Hz, 4H); ^{13}C NMR (101 MHz, DMSO-*d*6) δ 161.17, 142.62, 142.49, 139.69, 139.58, 138.85, 137.73, 130.04, 127.47, 121.81, 121.64, 120.96, 120.42, 108.26, 104.86, 100.61, 66.70, 62.54, 55.73, 53.68.

*4.1.2.7 (E)-3-(3,5-Dimethoxystyryl)-6-(6-(4-methylpiperazin-1-yl)pyridin-3-yl)-1H-indazole (**2f**).* Pale-yellow solid (yield 17.9%). HRMS (ESI-TOF) *m*/*z* calcd for $C_{27}H_{29}N_5O_2$ $[M + H]^+$: 456.2395, found: 456.2393; ^{1}H NMR (400 MHz, DMSO-d_6) δ 13.18 (s, 1H), 8.54 (d, J = 2.6 Hz, 1H), 8.24 (d, J = 8.5 Hz, 1H), 7.95 (dd, J = 8.9, 2.6 Hz, 1H), 7.68 (s, 1H), 7.57 (d, J = 16.6 Hz, 1H), 7.51–7.42 (m, 2H), 7.02–6.86 (m, 3H), 6.44 (t, J = 2.2 Hz, 1H), 3.81 (s, 6H), 3.56 (dd, J = 7.1, 3.1 Hz, 4H), 2.43 (t, J = 5.0 Hz, 4H), 2.24 (s, 3H); ^{13}C NMR (101 MHz, DMSO-d_6) δ 161.16, 158.80, 146.37, 142.59, 139.70, 136.66, 136.45, 129.96, 125.50, 121.85, 121.68, 120.26, 120.04, 107.49, 107.03, 104.86, 100.58, 55.73, 54.81, 46.23, 45.05.

*4.1.2.8 (E)-3-(3,5-Dimethoxystyryl)-6-(6-(piperazin-1-yl)pyridin-3-yl)-1H-indazole (**2g**).* Light grey solid (yield 29.1%). HRMS (ESI-TOF) *m*/*z* calcd for $C_{26}H_{27}N_5O_2$ $[M + H]^+$:442.2239, found: 442.2239; ^{1}H NMR (400 MHz, DMSO-d_6) δ 13.25 (s, 1H), 8.59 (d, J = 2.6 Hz, 1H), 8.29 (d, J = 8.5 Hz, 1H), 8.05–7.95 (m, 1H), 7.73 (s, 1H), 7.62 (d, J = 16.8 Hz, 1H), 7.57–7.46 (m, 2H), 6.97 (d, J = 2.4 Hz, 3H), 6.49 (t, J = 2.3 Hz, 1H), 3.87 (s, 6H), 3.54 (t, J = 4.7 Hz, 4H), 2.96–2.77 (m, 4H), 1.28 (s, 1H); ^{13}C NMR (101 MHz, DMSO-d_6) δ 161.16, 146.35, 142.67, 142.51, 139.70, 136.58, 136.50, 129.96, 125.22, 121.84, 121.62, 120.25, 120.00, 107.31, 107.03, 104.85, 100.58, 55.73, 46.24, 45.82.

*4.1.2.9 tert-Butyl (E)-4-(5-(3-(3,5-dimethoxystyryl)-1H-indazol-6-yl)pyridin-2-yl)piperazine-1-carboxylate (**2h**).* Light brown solid (yield 18.3%). HRMS (ESI-TOF) *m*/*z* calcd for $C_{31}H_{35}N_5O_4$ $[M + Na]^+$: 564.2582, found: 564.2594; ^{1}H NMR (400 MHz, DMSO-d_6) δ 13.19 (s, 1H), 8.56 (d, J = 2.6 Hz, 1H), 8.24 (d, J = 8.5 Hz, 1H), 7.98 (dd, J = 8.9, 2.6 Hz, 1H), 7.71–7.66 (m, 1H), 7.57 (d, J = 16.7 Hz, 1H), 7.51–7.43 (m, 2H), 6.96 (d, J = 8.9 Hz, 1H), 6.92 (d, J = 2.2 Hz, 2H), 6.44 (t, J = 2.2 Hz, 1H), 3.81 (s, 6H), 3.57 (dd, J = 6.9, 3.7 Hz, 4H), 3.46 (dd, J = 6.6, 3.8 Hz, 4H), 1.44 (s, 9H); ^{13}C NMR (101 MHz, DMSO-d_6) δ 161.16, 150.93, 142.68, 142.56, 139.73, 138.97, 138.23, 130.81, 129.88, 128.08, 121.77, 121.64, 120.57, 120.37, 119.88, 115.98, 107.04, 104.83, 100.57, 55.73, 55.02, 48.28, 46.26.

*4.1.2.10 (E)-4-(5-(3-(3,5-Dimethoxystyryl)-1H-indazol-6-yl) pyridin-2-yl)morpholine (**2i**).* Offwhite solid (yield 31.1%). HRMS (ESI-TOF) *m*/*z* calcd for $C_{26}H_{26}N_4O_3$ $[M + H]^+$: 443.2079, found: 443.2081; ^{1}H NMR (400 MHz, DMSO-d_6) δ 13.19 (s, 1H), 8.57 (d, J = 2.6 Hz, 1H), 8.24 (d, J = 8.5 Hz, 1H), 7.98 (dd, J = 8.8, 2.6 Hz, 1H), 7.69 (t, J = 1.0 Hz, 1H), 7.57 (d, J = 16.7 Hz, 1H), 7.50–7.43 (m, 2H), 7.01–6.85 (m, 3H), 6.44 (t, J = 2.2 Hz, 1H), 3.81 (s, 6H), 3.77–3.70 (m, 4H), 3.57–3.46 (m, 4H); ^{13}C NMR (101 MHz, DMSO-d_6) δ 161.16, 158.94, 146.29, 142.58, 142.56, 139.69, 136.75, 136.35, 129.99, 126.00, 121.87, 121.63, 120.30, 120.07, 107.51, 107.15, 104.86, 100.58, 66.43, 55.73, 45.64.

*4.1.2.11 (E)-3-(3,5-Dimethoxystyryl)-6-(2-(4-ethylpiperazin-1-yl)pyrimidin-5-yl)-1H-indazole (**2k**).* Light grey solid (yield 18.5%). HRMS (ESI-TOF) *m*/*z* calcd for $C_{27}H_{30}N_6O_2$ $[M + H]^+$: 471.2504, found: 471.2503; ^{1}H NMR (400 MHz, DMSO-d_6) δ 13.24 (s, 1H), 8.80 (s, 2H), 8.26 (d, J = 8.5 Hz, 1H), 7.73 (s, 1H), 7.57 (d, J = 16.7 Hz, 1H), 7.51–7.43 (m, 2H), 6.92 (d, J = 2.2 Hz, 2H), 6.44 (d, J = 2.3 Hz, 1H), 3.81 (s, 10H), 2.46 (s, 4H), 2.39 (d, J = 7.4 Hz, 2H), 1.05 (t, J = 7.1 Hz, 3H); ^{13}C NMR (101 MHz, DMSO-d_6) δ 161.16, 161.01, 156.63, 142.66, 142.46, 139.66, 133.72, 130.06, 122.72, 122.04, 121.54, 120.27, 119.89, 107.08, 104.88, 100.58, 55.73, 52.55, 52.10, 43.90, 12.28.

*4.1.2.12 (E)-3-(2,6-Dichloro-3,5-dimethoxystyryl)-6-(6-(4-methylpiperazin-1-yl)pyridin-3-yl)-1H-indazole (**2o**).* Pale-yellow solid (yield 24.4%). HRMS (ESI-TOF) *m*/*z* calcd for $C_{27}H_{27}Cl_2N_5O_2$ $[M + H]^+$: 524.1616, found: 524.1616; ^{1}H NMR (400 MHz, DMSO-d_6) δ 13.32 (s, 1H), 8.54 (d, J = 2.6 Hz, 1H), 8.10 (d, J = 8.5 Hz, 1H), 7.95 (dd, J = 8.9, 2.6 Hz, 1H), 7.75–7.70 (m, 1H), 7.51 (dd, J = 8.5, 1.5 Hz, 1H), 7.45 (d, J = 16.9 Hz, 1H), 7.38 (d, J = 17.0 Hz, 1H), 6.99–6.90 (m, 2H), 3.96 (s, 6H), 3.56 (t, J = 5.0 Hz, 4H), 2.42 (t, J = 5.0 Hz, 4H), 2.23 (s, 3H); ^{13}C NMR (101 MHz, DMSO-d_6) δ 158.81, 154.94, 148.73, 146.37, 142.68, 136.63, 135.54, 129.66, 125.35, 124.22, 121.31, 120.81, 119.83, 114.25, 112.98, 107.50, 107.19, 97.86, 57.18, 54.79, 46.21, 45.03.

4.1.3 Preparation of 3-(3,5-dimethoxyphenethyl)-6-(6-(4-methylpiperazin-1-yl)pyridin-3-yl)-1*H*-indazole (2p). To a solution of **2f** (0.1 mmol, 1.0 equiv) in methanol (10 mL) was added Pd/C (0.15 mmol, 1.5 equiv). The mixture was stirred at room temperature under H_2 atmosphere. When the reaction was complete detected by TLC, the solvent was concentrated under vacuum. The residue was dissolved in ethyl acetate and filtered with silica. The filtrate was washed with water and dried over anhydrous sodium sulfate. After concentrated, the crude product was purified by preparative thin layer chromatography to afford **2p**. Pale-yellow solid (yield 57.1%). HRMS (ESI-TOF) *m*/*z* calcd for $C_{27}H_{31}N_5O_2$ $[M + H]^+$:458.2552, found: 458.2548; ^{1}H NMR (400 MHz, DMSO-d_6) δ 12.67 (s, 1H), 8.49 (d, J = 2.6 Hz, 1H), 7.90 (dd, J = 8.9, 2.6 Hz, 1H), 7.79 (d, J = 8.4 Hz, 1H), 7.58 (d, J = 1.3 Hz, 1H), 7.32 (dd, J = 8.4, 1.5 Hz, 1H), 6.93 (d, J = 8.9 Hz, 1H), 6.46 (d, J = 2.3 Hz, 2H), 6.31 (t, J = 2.3 Hz, 1H), 3.70 (s, 6H), 3.54 (t, J = 5.1 Hz, 4H), 3.24–3.16 (m, 2H), 3.04–2.96 (m, 2H), 2.41 (t, J = 5.1 Hz, 4H), 2.23 (s, 3H); ^{13}C NMR (101 MHz, DMSO-d_6) δ 160.81, 158.74, 146.27, 144.98, 144.42, 142.13, 136.62, 136.07, 125.85, 121.04, 118.97, 107.48, 106.92, 106.73, 98.27, 55.48, 54.82, 46.25, 45.08, 35.37, 28.75.

4.1.4 Preparation of intermediates 2-6–2-13

*4.1.4.1 5-(1H-Indazol-6-yl)pyridin-2-amine (**2-6**).* 5-Bromopyridin-2-amine (20 mmol, 1.0 equiv.), (1*H*-indazol-6-yl) boronic acid (24 mmol, 1.2 equiv.), Pd(dppf)Cl_2 (1 mmol, 5 mol%) and potassium carbonate (30 mmol, 1.5 equiv.) were added to a mixed solvent of dioxane and H_2O (4 : 1, 50 mL). Then the reaction was heated to 100 °C and stirred overnight. The solvent was evaporated under reduced pressure, and the residue was dissolved in ethyl acetate, then filtered with silica. The filtrate was concentrated and purified by column chromatography to afford **2-6**. Light brown solid (yield 62.3%). MS *m*/*z* (ESI): 211.1 $[M + H]^+$.

*4.1.4.2 5-(1H-Indazol-6-yl)pyrimidin-2-amine (**2-7**).* The preparation of **2-7** was similar to **2-6**. Light brown solid (yield 59.7%). MS *m*/*z* (ESI): 212.0 $[M + H]^+$.

*4.1.4.3 4-(1H-Indazol-6-yl)pyridin-2-amine (**2-8**).* The preparation of **2-8** was similar to **2-6**. Light brown solid (yield 60.5%). MS *m*/*z* (ESI): 211.1 $[M + H]^+$; ^{1}H NMR (400 MHz, DMSO-d_6) δ 13.23 (s, 1H), 8.13 (s, 1H), 8.00 (d, J = 5.4 Hz, 1H), 7.86 (d, J = 8.4 Hz, 1H), 7.75 (s, 1H), 7.39 (d, J = 8.4 Hz, 1H), 6.94–6.74 (m, 2H), 6.05 (s, 2H).

*4.1.4.4 4-(1H-Indazol-6-yl)pyrimidin-2-amine (**2-9**).* The preparation of **2-9** was similar to **2-6**. Light brown solid (yield 56.0%). MS *m*/*z* (ESI): 212.1 $[M + H]^+$; ^{1}H NMR (400 MHz, DMSO-d_6) δ 13.17 (s, 1H), 8.41 (d, J = 5.2 Hz, 1H), 8.32 (d, J = 5.1 Hz, 1H), 8.10 (s, 1H) 7.86 (d, J = 8.6 Hz, 1H), 7.71 (d, J = 8.6 Hz, 1H), 7.64 (d, J = 5.3 Hz, 1H), 6.73 (s, 2H).

*4.1.4.5 5-(3-Iodo-1H-indazol-6-yl)pyridin-2-amine (**2-10**).* To a solution of intermediate **2-6** (10 mmol, 1.0 equiv) in DMF (15 mL) was added K_2CO_3 (20 mmol, 2 equiv) and iodine (15 mmol, 1.5 equiv) successively. After heated at 65 °C for 10 h, the mixture was poured into the aqueous solution of $Na_2S_2O_4$ and K_2CO_3, with a white solid precipitated. The solid was filtered and dried to give intermediate **2-10** as a white solid (yield 83.7%). MS *m*/*z* (ESI): 359.0 $[M + Na]^+$;

*4.1.4.6 5-(3-Iodo-1H-indazol-6-yl)pyrimidin-2-amine (**2-11**).* The preparation of **2-11** was similar to **2-10**. Offwhite solid (yield 85.0%). MS *m*/*z* (ESI): 359.0 $[M + Na]^+$;

*4.1.4.7 4-(3-Iodo-1H-indazol-6-yl)pyridin-2-amine (**2-12**).* The preparation of **2-12** was similar to **2-10**. Pale-yellow solid (yield 80.1%). MS *m*/*z* (ESI): 337.0 $[M + H]^+$.

*4.1.4.8 4-(3-Iodo-1H-indazol-6-yl)pyrimidin-2-amine (**2-13**).* The preparation of **2-13** was similar to **2-10**. Pale-yellow solid (yield 88.0%). MS *m*/*z* (ESI): 360.1 $[M + Na]^+$; ^{1}H NMR (400 MHz, DMSO-d_6) δ 13.20 (s, 1H), 8.30 (d, J = 5.0 Hz, 1H), 7.85 (d, J = 8.6 Hz, 1H); 7.66 (s, 1H), 7.41 (s, 1H), 6.79 (d, J = 5.1 Hz, 1H), 6.74 (s, 2H).

4.1.5 Preparation of compounds 2j, 2l, 2m and 2n

*4.1.5.1 (E)-5-(3-(3,5-Dimethoxystyryl)-1H-indazol-6-yl)pyridin-2-amine (**2j**).* The intermediates **2-10** (1 mmol, 1 equiv.) and **2-1** (1.2 mmol, 1.2 equiv.) was added to a mixed solvent of dioxane and H_2O (4 : 1, 15 mL), Pd(dppf)Cl_2 (0.05 mmol, 5 mol%) and cesium carbonate (2 mmol, 2.0 equiv.) was added as well. Then the reaction mixture was heated to 100 °C under N_2 atmosphere. After 8 h the solvent was evaporated under reduced pressure. The residue was dissolved in dichloromethane and methanol, and filtered with silica. The filtrate was concentrated and purified by preparative thin layer chromatography to give compound **2j** as a pale-yellow solid (yield 12.8%). HRMS (ESI-TOF) *m*/*z* calcd for $C_{22}H_{20}N_4O_2$ $[M + H]^+$: 373.1660, found: 373.1659; ^{1}H NMR (400 MHz, DMSO-d_6) δ 13.14 (s, 1H), 8.34 (d, J = 2.4 Hz, 1H), 8.22 (d, J = 8.5 Hz, 1H), 7.80 (dd, J = 8.6, 2.6 Hz, 1H), 7.64–7.53 (m, 2H), 7.50–7.40 (m, 2H), 6.92 (d, J = 2.3 Hz, 2H), 6.58 (d, J = 8.6 Hz, 1H), 6.44 (d, J = 2.3 Hz, 1H), 6.11 (s, 2H), 3.81 (s, 6H); ^{13}C NMR (101 MHz, DMSO-d_6) δ 161.16, 159.60, 146.36, 142.64, 142.58, 139.70, 136.95, 136.45, 129.91, 124.60, 121.76, 121.69, 120.15, 108.63, 106.65, 104.83, 100.58, 99.98, 55.73.

*4.1.5.2 (E)-5-(3-(3,5-Dimethoxystyryl)-1H-indazol-6-yl) pyrimidin-2-amine (**2l**).* The preparation of **2l** was similar to **2j**. Light brown solid (yield 30.1%). HRMS (ESI-TOF) *m*/*z* calcd for $C_{21}H_{19}N_5O_2$ $[M + H]^+$: 374.1613, found: 374.1611; ^{1}H NMR (400 MHz, DMSO-d_6) δ 13.21 (s, 1H), 8.67 (s, 2H), 8.25 (d, J = 8.5 Hz, 1H), 7.69 (s, 1H), 7.57 (d, J = 16.6 Hz, 1H), 7.50–7.43 (m, 2H), 6.92 (d, J = 2.2 Hz, 2H), 6.80 (s, 2H), 6.43 (t, J = 2.2 Hz, 1H), 3.81 (s, 6H); ^{13}C NMR (101 MHz, DMSO-d_6) δ 163.41, 161.16, 156.81, 153.71, 142.49, 139.68, 134.10, 130.00, 122.82, 121.98, 121.57, 120.17, 119.79, 106.82, 104.87, 100.60, 55.73.

*4.1.5.3 (E)-4-(3-(3,5-Dimethoxystyryl)-1H-indazol-6-yl)pyridin-2-amine (**2m**).* The preparation of **2m** was similar to **2j**. Light brown solid (yield 27.5%). HRMS (ESI-TOF) *m*/*z* calcd for $C_{22}H_{20}N_4O_2$ $[M + H]^+$: 373.1660, found: 373.1660; ^{1}H NMR (400 MHz, DMSO-d_6) δ 13.33 (s, 1H), 8.31 (d, J = 8.5 Hz, 1H), 8.01 (d, J = 5.3 Hz, 1H), 7.76 (s, 1H), 7.61 (d, J = 16.7 Hz, 1H), 7.54–7.43 (m, 2H), 6.94 (d, J = 2.2 Hz, 2H), 6.89 (dd, J = 5.4, 1.6 Hz, 1H), 6.82 (d, J = 1.6 Hz, 1H), 6.45 (t, J = 2.2 Hz, 1H), 6.03 (s, 2H), 3.82 (s, 6H); ^{13}C NMR (101 MHz, DMSO-d_6) δ 161.16, 160.91, 148.95, 148.88, 142.70, 142.25, 139.64, 137.19, 130.18, 121.98, 121.46, 121.19, 120.31, 110.93, 108.46, 105.96, 104.87, 100.65, 55.73.

*4.1.5.4 (E)-4-(3-(3,5-Dimethoxystyryl)-1H-indazol-6-yl) pyrimidin-2-amine (**2n**).* The preparation of **2n** was similar to **2j**. Light brown solid (yield 29.7%). HRMS (ESI-TOF) *m*/*z* calcd for $C_{21}H_{19}N_5O_2$ $[M + H]^+$: 374.1613, found: 374.1613; ^{1}H NMR (400 MHz, DMSO-d_6) δ 13.42 (s, 1H), 8.35 (d, J = 5.2 Hz, 1H), 8.33–8.22 (m, 2H), 7.90 (dd, J = 8.6, 1.4 Hz, 1H), 7.61 (d, J = 16.7 Hz, 1H), 7.49 (d, J = 16.7 Hz, 1H), 7.25 (d, J = 5.2 Hz, 1H), 6.93 (d, J = 2.3 Hz, 2H), 6.73 (s, 2H), 6.44 (t, J = 2.3 Hz, 1H), 3.82 (s, 6H); ^{13}C NMR (101 MHz, DMSO-d_6) δ 164.28, 164.08, 161.16, 159.59, 142.76, 142.03, 139.61, 135.65, 130.21, 122.31, 121.49, 121.36, 120.02, 109.27, 106.72, 104.90, 100.67, 55.74.

4.2 Biology experiments

4.2.1 Reagents. The Annexin V-FITC Apoptosis Detection Kit was purchased from KeyGen Biotech (Nanjing, China). Dimethyl sulfoxide (DMSO), rhodamine-123 (Rh123), 2′,7′-dichlorodihydrofluorescein diacetate (DCFH-DA) and 3-(4,5-dimethylthiazol-2-yl)-2,5-diphenyltetrazoliumbromide (MTT) were purchased from Sigma Chemical Co. (St Louis, MO, USA). 0.5% crystal violet was bought from Beyotime (Beijing, China). The primary antibodies against MMP9, cleaved caspase-3, Bax and Bcl-2 were obtained from Cell Signalling Technology (Beverly, MA, USA). β-Actin was purchased from ZSJQ-BIO Co.

(Beijing, China). Anti-Ki-67 mouse monoclonal was purchased from Merck Millipore (Billerica, MA, USA).

4.2.2 Cell lines and cell culture. The human cancer cell lines, A549, HepG2, MCF-4, and HCT116, as well as murine breast cancer cell line 4T1 were purchased from the American Type Culture Collection (Rockville, MD, USA). All cells were propagated in RPMI 1640 or DMEM media containing 10% heat-inactivated fetal bovine serum (FBS; Hyclone, Logan, UT, USA) and 1% antibiotics (penicillin and streptomycin) in 5% CO_2 at 37 °C.

4.2.3 Cell viability assay. Cells in logarithmic phase were seeded into 96-well culture plates at densities of 3000–5000 cells per well and incubated for 24 h. Then they were treated with different concentrations of compounds for various timings, 20 μL of MTT (5 mg mL^{-1}) was added to each well, and the cells were incubated for an additional 2–4 h. After carefully removal of the medium, the precipitates were dissolved in 150 μL of DMSO *via* mechanically shaking, and absorbance values were measured at a wavelength of 570 nm using a Spectra MAX M5 microplate spectrophotometer (Molecular Devices, Sunnyvale, CA, USA). The data presented are representative of three independent experiments.

4.2.4 Colony formation assay. In brief, 4T1 cells were seeded at a specified number (400–600 cells per well) in 6-well plates. After 24 h incubation, the cells were treated with various concentrations of **2f** (0–1.25 μM). The fresh medium with or without **2f** was changed every three days. After treatment for 10 days, the cells were washed with cold PBS, and the colonies were fixed with methanol and stained with a 0.5% crystal violet solution for 15 min, and the colonies (<50 cells) were counted under a microscope.

4.2.5 Apoptotic assay. Briefly, 4T1 cells (1–2 × 10^5 cells per well) were seeded in a 6-well plate overnight and treated with **2f**. After 24 h treatment, the cells were harvested and washed twice with PBS. The apoptosis levels were determined using an Annexin V-FITC apoptosis detection kit according to manufacturer's instructions by flow cytometry (FCM) (BD Biosciences). Data were analyzed using FlowJo software.

4.2.6 Western blot analysis. 4T1 cells were treated with **2f** in different concentration for 24 h, then cells were washed with cold PBS twice and lysed in RIPA buffer. The protein concentrations were examined using the Lowry method and equalized before loading. Equal amounts of protein from each sample were separated on 12% SDS-PAGE gel and transferred onto polyvinylidene fluoride (PVDF) membranes (Amersham Bioscience, Piscataway, NJ). The membranes were incubated with specific primary antibodies overnight at 4 °C. After incubation with the relevant secondary antibodies for 1 h, the reactive bands were identified using an enhanced chemiluminescence kit (Amersham). Then, the images were analyzed using the Image J computer software (National Institute of Health, Bethesda, MD, USA).

4.2.7 Mitochondrial membrane potential ($\Delta\Psi$m) assay. 2-(6-Amino-3-imino-3*H*-xanthen-9-yl) benzoic acid methyl ester (Rh123) was used to determine the changes in $\Delta\Psi$m by FCM. After the treatment with **2f** for 24 h, the harvested cells were incubated with Rh123 solution (5 μg mL^{-1}) at 37 °C for 30 min in the dark and $\Delta\Psi$m was then measured by FCM.

4.2.8 Measurement of ROS levels in cells. Briefly, after treatment with **2f** for 24 hours, 4T1 cells were treated with PBS containing 10 μM DCFH-DA. After incubation for 30 min at 37 °C, cells were washed twice with PBS, and then the ROS levels were detected by FCM.

4.2.9 Wound-healing migration assay. When cancer cells grew to about 80% confluence, the cell monolayer was scraped with sterile 100 μL pipette tips, and fresh medium containing different concentrations of **2f** was added. After 24 h incubation, cells were fixed and photographed using a microscope (Zeiss, Jena, Germany). The migrated cells were quantified by manual counting using 100% as the value assigned for the vehicle group.

4.2.10 Boyden chamber migration and invasion assay. The Boyden chamber (8 μm pore size) migration assay was performed as previously described but with some modifications.[36] Briefly, a total of 5 × 10^4 4T1 cells in 100 μL serum-free medium were added in the top chamber, and 600 μL of medium containing 10% FBS was added to the bottom. Both chambers contained different concentrations of **2f**. Cells were allowed to migrate for 24 h. The migrated cells were fixed in 100% methanol and stained with 0.5% crystal violet. The migrated cells were quantified by manual counting and photographed under a light microscope. Invasion assay was performed according to previous reports.[36] Briefly, the upper surface of the transwell plate was preincubated with serum-free medium diluted Matrigel (1 : 1, 60 μL per well, BD Biosciences, USA). After Matrigel polymerization, the bottom chambers were filled with 600 μL medium containing 10% FBS. 5 × 10^4 4T1 cells in 100 μL serum-free medium were added in the top part of each transwell and treated with different concentrations of **2f**. After incubation for 24 h, non-migrated cells on the upper side of the filter were removed with a cotton swab, and migrated cells were fixed with 4% paraformaldehyde and stained with 0.5% crystal violet and counted under a light microscope. The percentage of migrated cells inhibited by **2f** was expressed on the basis of control wells.

4.2.11 Mice, tumor model and treatment. All animal experiments were approved and conducted by the Institutional Animal Care and Treatment Committee of Sichuan University in China (Permit Number: 20181201-3). Six- to eight-week-old female BALB/c mice (Beijing HFK bioscience Co., Ltd, Beijing, China) were used in this study. 100 μL 4T1 tumor cell suspension containing 2 × 10^6 cells were injected subcutaneously in the right flank of BALB/c mice. When the tumor tissue grows to about 400 mm^3, the tumor-bearing mice were randomized into three groups (5 mice per group), and received intraperitoneally injection (i.p.) of **2f** 12.5 mg kg^{-1}, 25 mg kg^{-1} or vehicle, respectively once daily for 16 days. Tumor volumes and body weight were assessed every three days. The tumor size was calculated according to the formula: tumor volume ($m\ m^3$) = $0.52 \times a \times b^2$ where a is the length and b is the width.

4.2.12 Immunohistochemistry. One part of paraffin tumor sections was stained with hematoxylin and eosin (H&E). The other part was stained with Ki67, cleaved casepase-3, MMP9

antibodies using immunohistochemistry staining to investigate tumor cell proliferation, apoptosis and metastasis, respectively.

4.2.13 Toxicity evaluation. Blood was obtained for hematological and serum biochemistry analysis by Hitachi 7200 Blood Chemistry Analyzer and a Nihon Kohden MEK-5216K Automatic Hematology Analyzer. The tissues of heart, lung, spleen, liver and kidney were stained with H&E for histopathologic examination.

4.2.14 Statistical analysis. The data were expressed as the mean ± SD. The statistical comparisons were made by Student's *T* test and a statistically significant difference was considered to be present at $*p < 0.05$; $**p < 0.01$; $***p < 0.001$.

Author contributions

Wei Wei, Zhihao Liu and Tinghong Ye developed the idea for the study, performed the research, analyzed data and wrote the paper; Xiuli Wu, Cailing Gan, Xingping Su, Hongyao Liu Hanyun Que and Qianyu Zhang provided data; Qiang Xue and Lin Yue revised the manuscript; Luoting Yu and Tinghong Ye supervised the research, acquired funding and revised the manuscript. All authors have approved the final version of the manuscript.

Conflicts of interest

There are no conflicts to declare.

Acknowledgements

This work was supported by Shanghai pharmaceutical group co. LTD (16H0017), the Natural Science Foundation of China (No. 81903441), and Post-Doctor Research Project, West China Hospital, Sichuan University, China (No. 2018HXBH009). We thank Anne M. O'Rourke, PhD, from Liwen Bianji, Edanz Group China (www.liwenbianji.cn/ac), for editing the English text of a draft of this manuscript.

References

1 H. Sung, J. Ferlay, R. L. Siegel, M. Laversanne, I. Soerjomataram, A. Jemal and F. Bray, *Ca-Cancer J. Clin.*, 2021, DOI: 10.3322/caac.21660.
2 L. A. Emens, P. A. Ascierto, P. K. Darcy, S. Demaria, A. M. M. Eggermont, W. L. Redmond, B. Seliger and F. M. Marincola, *Eur. J. Cancer*, 2017, **81**, 116–129.
3 K. A. High and M. G. Roncarolo, *N. Engl. J. Med.*, 2019, **381**, 455–464.
4 K. D. Miller, L. Nogueira, A. B. Mariotto, J. H. Rowland, K. R. Yabroff, C. M. Alfano, A. Jemal, J. L. Kramer and R. L. Siegel, *Ca-Cancer J. Clin.*, 2019, **69**, 363–385.
5 L. Wan, K. Pantel and Y. Kang, *Nat. Med.*, 2013, **19**, 1450.
6 D. D. Gaikwad, A. D. Chapolikar, C. G. Devkate, K. D. Warad, A. P. Tayade, R. P. Pawar and A. J. Domb, *Eur. J. Med. Chem.*, 2015, **90**, 707–731.
7 I. Denya, S. F. Malan and J. Joubert, *Expert Opin. Ther. Pat.*, 2018, **28**, 441–453.
8 S. G. Zhang, C. G. Liang and W. H. Zhang, *Molecules*, 2018, **23**.
9 J. Dong, Q. Zhang, Z. Wang, G. Huang and S. Li, *ChemMedChem*, 2018, **13**, 1490–1507.
10 S. Yan, Y. Dong, Q. Peng, Y. Fan, J. Zhang and J. Lin, *RSC Adv.*, 2013, **3**, 5563–5569.
11 G. Sandeep Reddy, S. Mohanty, J. Kumar and B. Venteswar Rao, *Russ. J. Gen. Chem.*, 2018, **88**, 2394–2399.
12 P. A. Harris, A. Boloor, M. Cheung, R. Kumar, R. M. Crosby, R. G. Davis-Ward, A. H. Epperly, K. W. Hinkle, R. N. Hunter 3rd, J. H. Johnson, V. B. Knick, C. P. Laudeman, D. K. Luttrell, R. A. Mook, R. T. Nolte, S. K. Rudolph, J. R. Szewczyk, A. T. Truesdale, J. M. Veal, L. Wang and J. A. Stafford, *J. Med. Chem.*, 2008, **51**, 4632–4640.
13 S. Miyamoto, S. Kakutani, Y. Sato, A. Hanashi, Y. Kinoshita and A. Ishikawa, *Jpn. J. Clin. Oncol.*, 2018, **48**, 503–513.
14 B. W. Konicek, A. R. Capen, K. M. Credille, P. J. Ebert, B. L. Falcon, G. L. Heady, B. K. R. Patel, V. L. Peek, J. R. Stephens, J. A. Stewart, S. L. Stout, D. E. Timm, S. L. Um, M. D. Willard, I. H. Wulur, Y. Zeng, Y. Wang, R. A. Walgren and S. C. Betty Yan, *Oncotarget*, 2018, **9**, 13796–13806.
15 S. B. Yan, S. L. Um, V. L. Peek, J. R. Stephens, W. Zeng, B. W. Konicek, L. Liu, J. R. Manro, V. Wacheck and R. A. Walgren, *Invest. New Drugs*, 2018, **36**, 536–544.
16 A. R. He, R. B. Cohen, C. S. Denlinger, A. Sama, A. Birnbaum, J. Hwang, T. Sato, N. Lewis, M. Mynderse, M. Niland, J. Giles, J. Wallin, B. Moser, W. Zhang, R. Walgren and E. R. Plimack, *Oncologist*, 2019, **24**, e930–e942.
17 Z. T. Al-Salama and S. J. Keam, *Drugs*, 2019, **79**, 1477–1483.
18 Y. Umeyama, Y. Shibasaki and H. Akaza, *Future Oncol.*, 2017, **13**, 1839–1852.
19 A. Bellesoeur, E. Carton, J. Alexandre, F. Goldwasser and O. Huillard, *Drug Des., Dev. Ther.*, 2017, **11**, 2801–2811.
20 G. Zhao, W. Y. Li, D. Chen, J. R. Henry, H. Y. Li, Z. Chen, M. Zia-Ebrahimi, L. Bloem, Y. Zhai, K. Huss, S. B. Peng and D. J. McCann, *Mol. Cancer Ther.*, 2011, **10**, 2200–2210.
21 M. Michael, Y. J. Bang, Y. S. Park, Y. K. Kang, T. M. Kim, O. Hamid, D. Thornton, S. C. Tate, E. Raddad and J. Tie, *Target. Oncol.*, 2017, **12**, 463–474.
22 J. M. Mason, D. C. Lin, X. Wei, Y. Che, Y. Yao, R. Kiarash, D. W. Cescon, G. C. Fletcher, D. E. Awrey, M. R. Bray, G. Pan and T. W. Mak, *Cancer Cell*, 2014, **26**, 163–176.
23 P. B. Sampson, Y. Liu, B. Forrest, G. Cumming, S. W. Li, N. K. Patel, L. Edwards, R. Laufer, M. Feher, F. Ban, D. E. Awrey, G. Mao, O. Plotnikova, R. Hodgson, I. Beletskaya, J. M. Mason, X. Luo, V. Nadeem, X. Wei, R. Kiarash, B. Madeira, P. Huang, T. W. Mak, G. Pan and H. W. Pauls, *J. Med. Chem.*, 2015, **58**, 147–169.
24 Y. Zhao and X. Wang, *J. Cancer Res. Clin. Oncol.*, 2019, **145**, 2413–2422.
25 Combination Merestinib and LY2874455 for Patients With Relapsed or Refractory Acute Myeloid Leukemia, https://www.clinicaltrials.gov/ct2/show/NCT03125239?term=NCT03125239&draw=2&rank=1, accessed Feb. 9, 2020.
26 CFI-400945 in Patients With Advanced/Metastatic Breast Cancer, https://www.clinicaltrials.gov/ct2/show/

NCT03624543?term=NCT03624543&draw=2&rank=1, accessed Feb. 9, 2021.

27 R. Sheng, S. Li, G. Lin, S. Shangguan, Y. Gu, N. Qiu, J. Cao, Q. He, B. Yang and Y. Hu, *RSC Adv.*, 2015, **5**, 81817–81830.

28 L. Yang, Y. Chen, J. He, E. M. Njoya, J. Chen, S. Liu, C. Xie, W. Huang, F. Wang, Z. Wang, Y. Li and S. Qian, *Bioorg. Med. Chem.*, 2019, **27**, 1087–1098.

29 L. N. Solano, G. L. Nelson, C. T. Ronayne, S. Jonnalagadda, S. K. Jonnalagadda, K. Kottke, R. Chitren, J. L. Johnson, M. K. Pandey, S. C. Jonnalagadda and V. R. Mereddy, *Sci. Rep.*, 2020, **10**, 17969.

30 R. Laufer, B. Forrest, S.-W. Li, Y. Liu, P. Sampson, L. Edwards, Y. Lang, D. E. Awrey, G. Mao, O. Plotnikova, G. Leung, R. Hodgson, I. Beletskaya, J. M. Mason, X. Luo, X. Wei, Y. Yao, M. Feher, F. Ban, R. Kiarash, E. Green, T. W. Mak, G. Pan and H. W. Pauls, *J. Med. Chem.*, 2013, **56**, 6069–6087.

31 P. B. Sampson, Y. Liu, N. K. Patel, M. Feher, B. Forrest, S.-W. Li, L. Edwards, R. Laufer, Y. Lang, F. Ban, D. E. Awrey, G. Mao, O. Plotnikova, G. Leung, R. Hodgson, J. Mason, X. Wei, R. Kiarash, E. Green, W. Qiu, N. Y. Chirgadze, T. W. Mak, G. Pan and H. W. Pauls, *J. Med. Chem.*, 2015, **58**, 130–146.

32 J. Liu, X. Peng, Y. Dai, W. Zhang, S. Ren, J. Ai, M. Geng and Y. Li, *Org. Biomol. Chem.*, 2015, **13**, 7643–7654.

33 B. Zhao, Y. Li, P. Xu, Y. Dai, C. Luo, Y. Sun, J. Ai, M. Geng and W. Duan, *ACS Med. Chem. Lett.*, 2016, **7**, 629–634.

34 J. Cui, X. Peng, D. Gao, Y. Dai, J. Ai and Y. Li, *Bioorg. Med. Chem. Lett.*, 2017, **27**, 3782–3786.

35 Z. Liu, Q. Lei, W. Wei, L. Xiong, Y. Shi, G. Yan, C. Gao, T. Ye, N. Wang and L. Yu, *RSC Adv.*, 2017, **7**, 27737–27746.

36 T. Ye, X. Wei, T. Yin, Y. Xia, D. Li, B. Shao, X. Song, S. He, M. Luo, X. Gao, Z. He, C. Luo, Y. Xiong, N. Wang, J. Zeng, L. Zhao, G. Shen, Y. Xie, L. Yu and Y. Wei, *Breast Cancer Res. Treat.*, 2014, **143**, 435–446.